Fabric domains in quartz mylonites: localized three dimensional analysis of microstructure and texture

CHRISTIAN PAULI, STEFAN M. SCHMID and RENÉE PANOZZO HEILBRONNER*

Geologisch-Paläontologisches Institut, Universität Basel, Bernoullistrasse 32, CH-4056 Basel,
Switzerland

Abstract—Fabric domains of a quartz vein deformed under greenschist facies conditions are analysed with domainal X-ray texture goniometry, optical microscopy, computer integrated polarization microscopy (CIP) and shape analysis in two mutually perpendicular sections. The analysed domains consist of large non-recrystallized deformed clast fragments, prolate non-recrystallized ribbon grains and prolate recrystallized domains. In terms of texture, monomaximal and polymaximal domains have been distinguished. Pronounced partitioning of deformation is observed between these domains. This strain partitioning asks for caution when making kinematic inferences for fault zones based on a study of domainal fabrics. Domains persist as fabric elements up to high strains. This emphasizes the often neglected role of a non-random initial fabric. Neighbouring domains with alternating c-axis orientations and grain boundary preferred orientations, indicating opposing senses of shear, occur in both sections.

The bulk texture is controlled by clast and ribbon domains, rather than being strictly deformation-induced. We infer that prolate elongation of clasts and ribbons is achieved mainly by combined prism and basal slip. Recrystallized domains are characterized by different textures. They are deformed by intracrystalline slip, combined with grain boundary migration and sliding. Inclined preferred grain boundary orientations are continuously maintained by grain boundary migration. Copyright © 1996 Elsevier Science Ltd

INTRODUCTION

Fabric studies in quartz mylonites are important for unraveling the kinematics of movement and deformation mechanisms in shear zones. In most cases such studies address the bulk fabric (microstructure and texture), the analysis of the sample being restricted to one single thin section. However, it was recognized earlier in this century, that microstructure and texture may be domainal within a specimen. The invention of the method of 'Achsenverteilungsanalysen' (AVA, axial distribution analysis) by Sander (1934a,b) allowed for both the direct visualization of fabric domains, i.e. areas with homogeneous texture and microstructure, and interrelations between microstructure and texture. Ramsauer (1941)also in Sander 1950) and Koark (1957) analysed AVA's of several sections of one sample and impressively documented three dimensional fabric domains. A number of more recent works (e.g. Wenk 1965, Hobbs 1966, Eisbacher 1970, Price 1978, Garcia Celma 1982, Passchier 1983, Knipe & Law 1987) also observed domainal rather than homogeneous fabrics on the scale of the thin section.

Fabric domains may originate from single large grains behaving as passive markers, their shape reflecting finite deformation, and their texture depending on the deformation mechanism. On the other hand grain boundary migration processes within domains as well as between domains ('domain boundary migration') may dominate (e.g. Knipe & Law 1987). Consequently, domains may behave as actively evolving and compet-

ing elements of the bulk specimen. In both cases the fabric evolution on the grain and domain scale plays a major role during deformation of the bulk sample (Lloyd *et al.* 1992).

AVA applications to quartz using optical methods discuss texture and fabric domains only in terms of c-axis orientation. Specific c-axis orientations in a stereogram are combined into direction groups ('Richtungsgruppen', Sander 1930, 1950, 1970), and the corresponding grains are coloured on a sketch of the microstructure. The interpretation of clusters of grains with equally oriented c-axes ('Feinlagen', Sander 1950) in terms of slip planes and slip directions in quartz were rather speculative at that time. However some key questions regarding the development of textures were addressed (e.g. Sander 1930, 1950, Schmidt 1932; see below) and linked to microstructural features. For example (Sander 1911, 1930, 1950), developed the concept of strain partitioning ('Teilbewegungen') within a rock body, individual displacements within domains not necessarily being controlled by bulk shortening and extension (Sander 1911, Turner & Weiss 1963). This approach implies that predictions of the bulk deformation from the analysis of deformation on a smaller (i.e. local) scale are not possible. Schmidt (1926, 1927a,b, 1932), on the other hand, interpreted quartz textures in terms of intracrystalline slip systems in quartz. He argued that the active slip plane and slip direction of the grains eventually are going to be aligned with the macroscopically observed slip plane and slip direction (e.g. Schmidt 1926, p. 424), neglecting possible effects of strain partitioning.

More recent empirical interpretations based on a 'Schmidt'-type approach (e.g. Bouchez 1978, Schmid & Casey 1986) and modeling of texture development (e.g. Lister *et al.* 1978, Wenk *et al.* 1989, Jessell & Lister 1990)

*Send correspondence to: Renée Panozzo Heilbronner, Geologisch-Paläontologisches Institut, Universität Basel, Bernoullistrasse 32, CH-4056 Basel, Switzerland. e-mail: heilbronner@ubaclu.unibas.ch

usually provide explanations of bulk texture patterns only. Interestingly, some texture models actually predict the evolution of domains (Etchecopar 1977, Gapais & Cobbold 1987). However, the interaction of fabric elements on the grain and domain scale and the interplay of plastic deformation with grain boundary migration and/or sliding processes are only rudimentarily taken into account by most modern studies. The works of Garcia Celma (1982), discussing fabric domains in terms of c-axis orientations, and of Lloyd et al. (1992), using the SEM electron channelling method capable of analysing the complete texture, are notable exceptions.

This study analyses textural and microstructural patterns of small scale fabric domains within a hetero-geneous monomineralic quartz sample in order to gain information on the domain-forming processes and on strain partitioning within the chosen sample. The fabric domains are characterized by integrating microstructural and textural analyses using recently developed techniques. Domainal texture goniometry provides information on crystal directions other than the c-axis within larger scale domains. Computer integrated polarization microscopy (CIP, Panozzo Heilbronner & Pauli 1993, 1994) reveals intimate relations between c-axis orientations and microstructure within smaller scale domains, analogous to the AVA technique. Image analysis (Panozzo 1983) quantifies microstructural features such as grain shapes and preferred boundary orientation and can be directly combined with the CIP method.

Emphasis is placed on the three-dimensional aspects of fabric domains by analysing two perpendicular sections of the same sample.

GEOLOGICAL SETTING AND SAMPLE DESCRIPTION

The sample analysed was taken from the Corvatsch mylonite zone, located in SE Switzerland (Fig. 1), which represents an extensional fault zone with top to the east sense of shear that formed during the collapse of the Austroalpine nappe pile in Late Cretaceous times (Liniger 1992). Mylonitization is contemporaneous with a marked pressure decrease from 8 to 6 kbar. In the more southern, structurally deeper parts of the fault zone deformation occurs under temperatures of about 400°C (Liniger 1992). In the higher parts Liniger (1992) and Fitz Gerald & Stünitz (1993) describe a mineral assemblage consisting of actinolite + chlorite + albite + epidote + clinozoisite + white mica ± stilpnomelane, typical for lower to mid-greenschist facies assemblages (300°C to 400°C at the time of deformation, Fitz Gerald & Stünitz 1993). Along the Corvatsch fault zone several generations of originally coarse-grained quartz veins can be distinguished, differing in their orientation, cross-cutting relations and amount of recorded deformation. Old veins, such as the specimen selected for this study, are isoclinally folded and boudinaged and are most abundant in crystalline slivers along the base of the Corvatsch nappe (Fig. 1).

The sample discussed here stems from a 5 cm thick quartz vein oriented parallel to the fault zone (inset of Fig. 1). The vein shows, on its interface with the country rock, a faint East-dipping lineation. Section A, cut parallel to the lineation and perpendicular to foliation (Fig. 2a), shows a pronounced lamination, which consists either of gray-translucent ribbon grains or of light gray recrystallized domains which appear milky in hand specimen. Within measuring errors layering, vein boundaries and foliation of the country rock are parallel to each other. Microscopic inspection shows that the milky appearance is due to abundant fluid inclusions in the recrystallized domains.

The macroscopically observable laminar structure of section A corresponds in thin section to large non-recrystallized quartz ribbons and partly to domains of recrystallized grains (Fig. 3a). Typically the domains are in excess of 20 mm long and 600 μm wide (aspect ratio at least 1:30). The recrystallized grain size is between 70 and 100 μm. Two thirds of the section is composed of c-axis orientations resulting in magenta colours with the lambda plate inserted (i.e. appearing gray in Fig. 3a). They are separated by thin trails of differently oriented grains. In the lower part of the section a quartz ribbon grain is boudinaged (arrow on Figs. 2a and 3a). Near the top border of the section similarly sized layers with dark gray (blue) and light gray (yellow) colours dominate.

Section B, cut perpendicular to the lineation and perpendicular to the foliation (Fig. 2b), consists of smaller lens shaped translucent areas corresponding to ribbon grains and of the elongated, lenticular light-gray to milky white streaks of recrystallized domains. In addition, a lenticular area with gray-translucent quartz fragments is visible. These fragments are separated by veins formed by recrystallized quartz grains (arrows in Figs. 2b and 3b). The ribbons in the laminar section A. clearly correspond to the lenticular ribbons and the clast fragments in section B. Assuming these non-recrystallized rod-shaped domains to represent strain markers, a constrictional strain is derived.

Microscopic inspection reveals ribbon grains in the upper half of section B (Fig. 3, grey areas in Fig. 2). They are 2 mm wide and 200–600 μm thick, yielding an aspect ratio of approximately 1:6. The thickness of the recrystallized domains ranges from 200 to 1000 μm. The recrystallized grain size is approximately 100 μm and the grains show a weak shape preferred orientation.

DEFINITIONS OF DOMAINS AND DIRECTION GROUPS

Fabric domains

Following Turner & Weiss (1963, p. 20) we define domains to specify finite three dimensional portions of a rock body which are statistically homogeneous on the scale of the domain. The term fabric denotes the microfabric in the sense of Hobbs et al. (1976), i.e. consisting of two complementary parts: the microstruc-
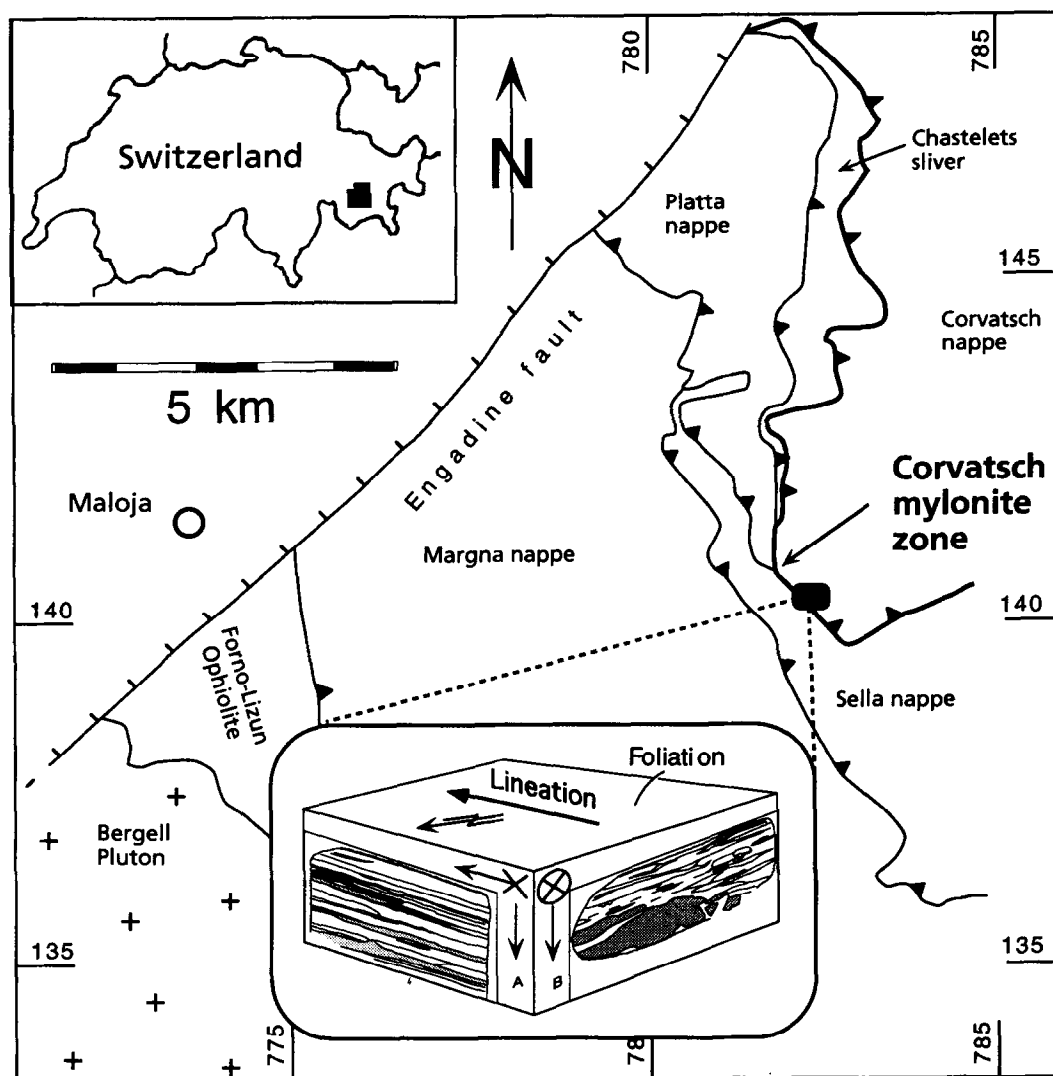
Fig. 1. Location of the Corvatsch mylonite zone, sampling location and specimen orientation (after Liniger 1992). Lineation is 094/04°. Sense of shear is sinistral (see text).

ture and the crystallographic preferred orientation (referred to as texture in this paper).

The size and definitions of the fabric domains analysed in this study depend on the method of analysis. Fabric domains defined by using a conventional optical microscope are regions with a similar c-axis orientation pattern as outlined in Fig. 2(a,b). The domain boundaries are based solely on the interference colours of the grains when viewed with crossed polarizers and the lambda plate inserted.

Using the texture goniometer, the size of fabric domains is given by the area scanned by the X-ray beam. These areas are denoted A and B, depending on the orientation of the section, and are provided with a suffix which defines the elongation of the sampling area: 'p' and 's' denote a scan parallel and perpendicular to foliation respectively. Note that these areas may well comprise a number of fabric domains as analysed by the other methods.

A third way of defining fabric domains is through the CIP analysis. We consider this the most satisfactory 'light optical' definition of domains. Generally, the CIP derived domains are smaller than those outlined in Fig. 2(a,b).

They are numbered in alphabetical order from top to bottom by letters that are appended to the section identifier (see e.g. Fig. 3). For example, A.B is the second domain counted from above in section A. There is no correspondence between domain letters of section A and B.

Direction groups

In order to interpret preferred c-axis orientations, the c-axis pole figure is subdivided into subareas, representing the so-called *direction groups*. Figure 4 defines the direction groups used in this study. The roman lettering is not identical to but closely similar to a convention used by Sander (1930, 1950) and Fairbairn (1949). The suffixes 'h' (hangingwall) and 'f' (footwall) denote direction groups II with respect to the foliation (horizontal in Fig. 4a). The peripheral groups III have an 's' (sinistral) or 'd' (dextral), denoting the sense of deflection with respect to the foliation normal (vertical in Fig. 4a). For ease of comparison of A- and B-sections the direction groups are also displayed on a rotated pole figure (Fig. 4b).
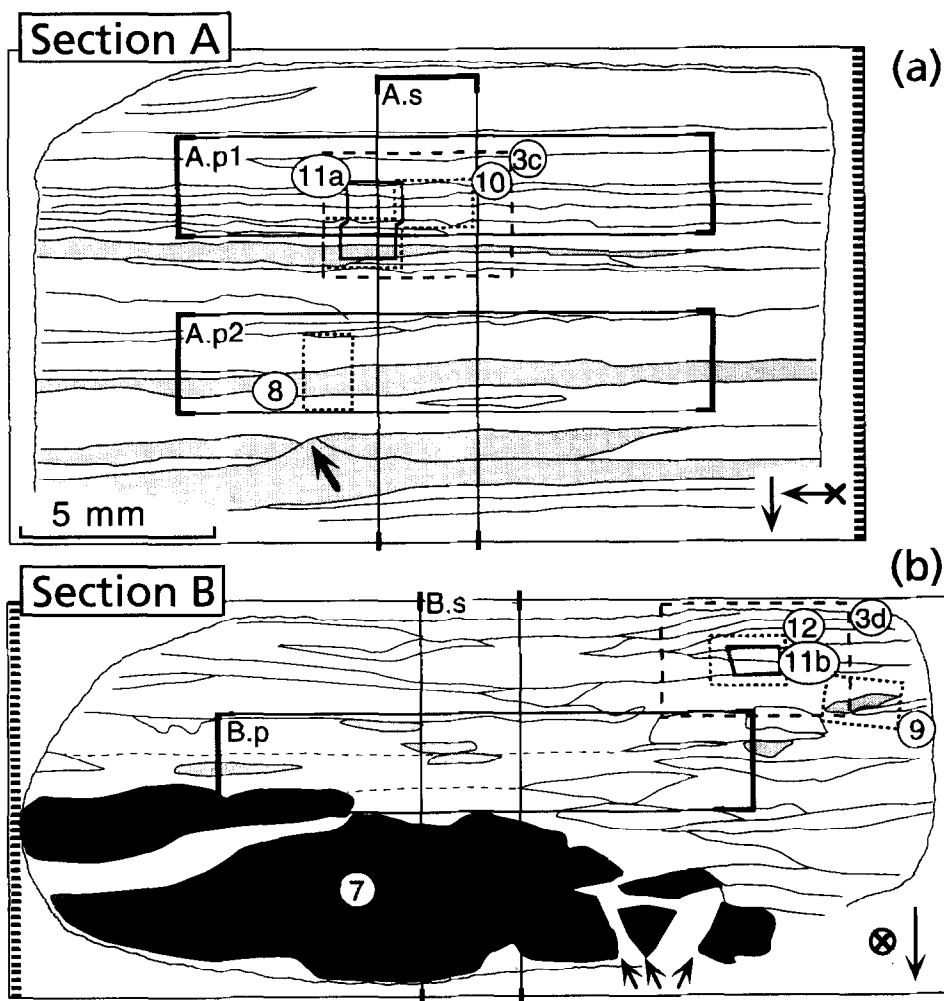
Fig. 2. Two orthogonal sections of mylonite sample. The common edge of the sections is indicated by heavy stipples. Rectangles with heavy handles delineate the measurement areas of the X-ray goniometry. Dashed rectangles delineate detailed micrographs. Stippled rectangles delineate areas of CIP-derived orientation images. Full lines delineate areas of shape analysis. Numbers refer to figures of this article. (a) Section A is cut parallel to the lineation. Recrystallized domains of roughly parallel c-axis orientation and ribbon grains (shaded) can be traced across the section. Arrow: necking of quartz ribbon grain. (b) Section B is cut perpendicular to the lineation. Domains appear more lenticular. Light gray: ribbon grains (cf. section A). Dark gray: quartz clast fragments.

The direction groups defined in Fig. 4 are used to define monomaximal and polymaximal fabric domains: monomaximal domains occupy one direction group, and polymaximal domains occupy more than one direction group. Polymaximal direction groups are thus characterized by one streaked out or several c-axis maxima. They also form the basis for defining colour look up tables (CLUTs) used for the colour coding of the orientation images (Panozzo Heilbronner & Pauli 1993, 1994).

TEXTURE GONIOMETRY

X-ray texture goniometry was used to complement the CIP-derived orientation images which are based on the c-axis orientation alone. We are aware that a full textural description of domains is only possible on the basis of full crystallographic orientations as provided by certain SEM techniques (see Lloyd & Freeman 1991, Kunze et al. 1993). Nevertheless, the combination of X-ray texture analysis and CIP is used here in order to cope with the

relatively large sample size that is necessary when studying domainal samples.

With modern texture goniometers it is possible to analyse an area that corresponds to just a few optically defused domains. An improved mounting technique offers the possibility of analysing the rectangular areas shown in Figs. 2(a,b) and Figs. 3(a,b). If scanned parallel to the foliation, the resulting texture is the composite of a few domains, if scanned perpendicular to the foliation, the beam crosses all domains and yields a bulk texture.

Two chips were analysed in a Siemens D5000-goniometer. Four peaks (a {1120}, m {1010}, r {1101} + z {0111}, {1014}) were measured up to an angle of 80 degrees in reflection mode. These incomplete pole figures were used as input into MENTEX, the entropy based ODF-calculation program package by Schaeben et al. (1990). Upper hemisphere pole figures for c- (<0001 >) and a, (<1120 >) directions, as well as the poles of m- {1010}, r- {1011} and z- {0111} planes were recalculated from the ODF. c-axis pole figures document the orientation of the basal plane. The m-, r- and z-planes are given
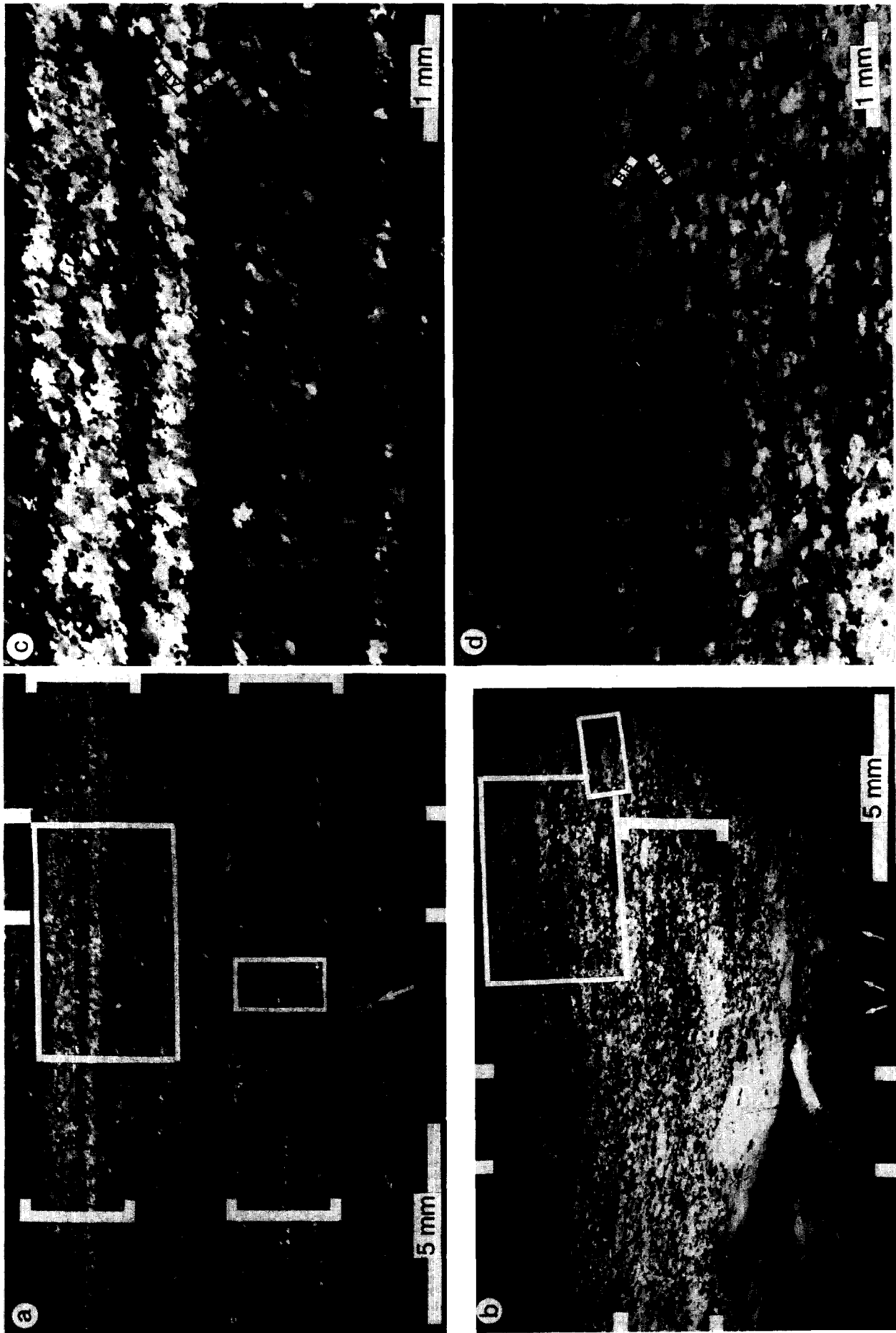
Fig. 3. Photomicrographs as depicted in Fig. 2 (crossed polarizers, lambda plate inserted with addition direction NW–SE). (a) Overview of thin section parallel to the lineation. Note elongated domainal microfabric. (b) Overview of thin section perpendicular to the lineation. Note lozenge shape of the domains, and large and distorted (arrows) quartz clast fragments in lower part. (c) Thin section parallel to the lineation. Herring bone microstructure indicated by domains A.B and A.C; ribbon grain R by domain A.G. (d) Thin section perpendicular to the lineation. Herring bone microstructure indicated by domains B.B and B.C.
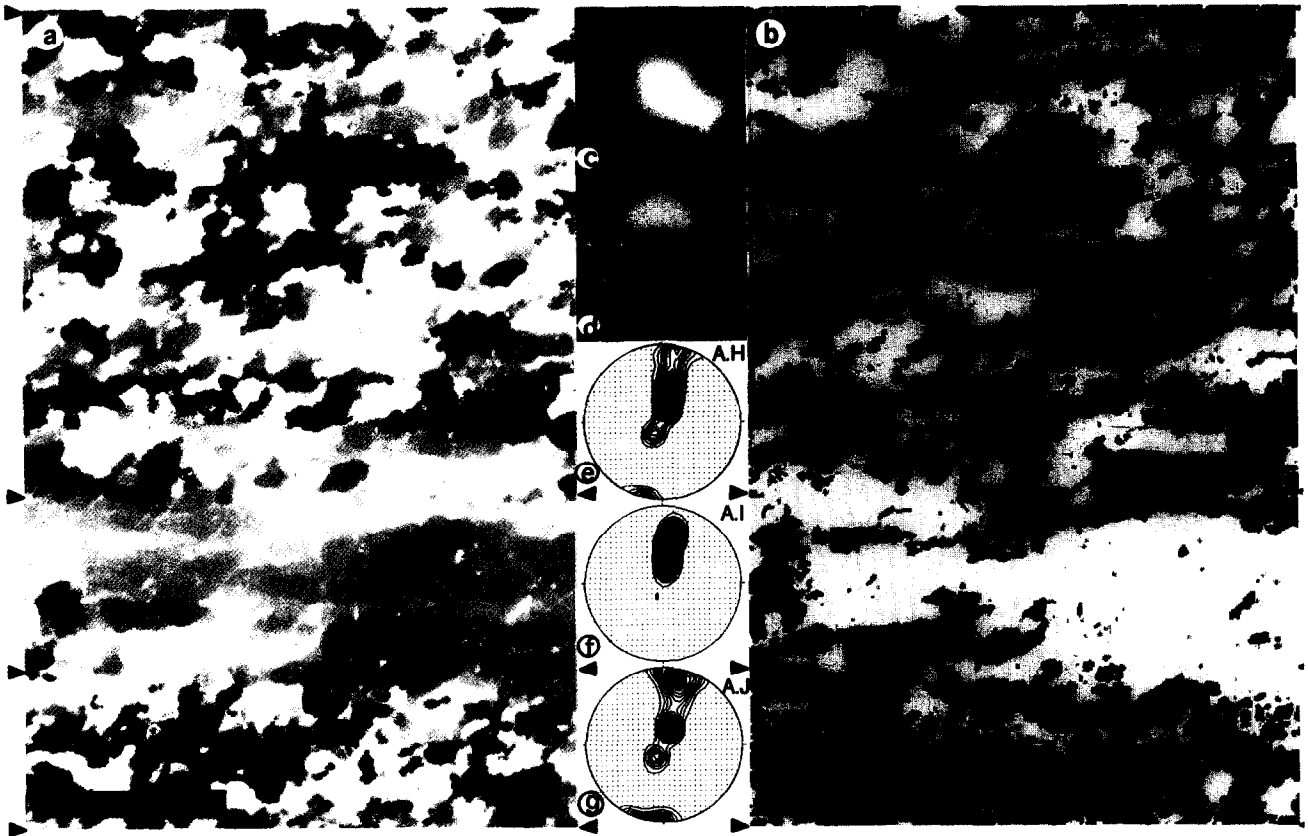
Fig. 8. CIP analysis of three domains of section A (A.H., A.I, A.J.). Domain boundaries are marked by triangles. See Fig. 2(a) for location in specimen. (a) Orientation image using standard CLUT (c) (see text). (b) Orientation image using problem adapted CLUT (d). (c) Standard colour look-up table (CLUT). (d) Problem adapted CLUT (for definition, see Fig. 4a). Volume weighted stereograms: (e) of domain A.H, (f) of domain A.I, and (g) of domain A.J.
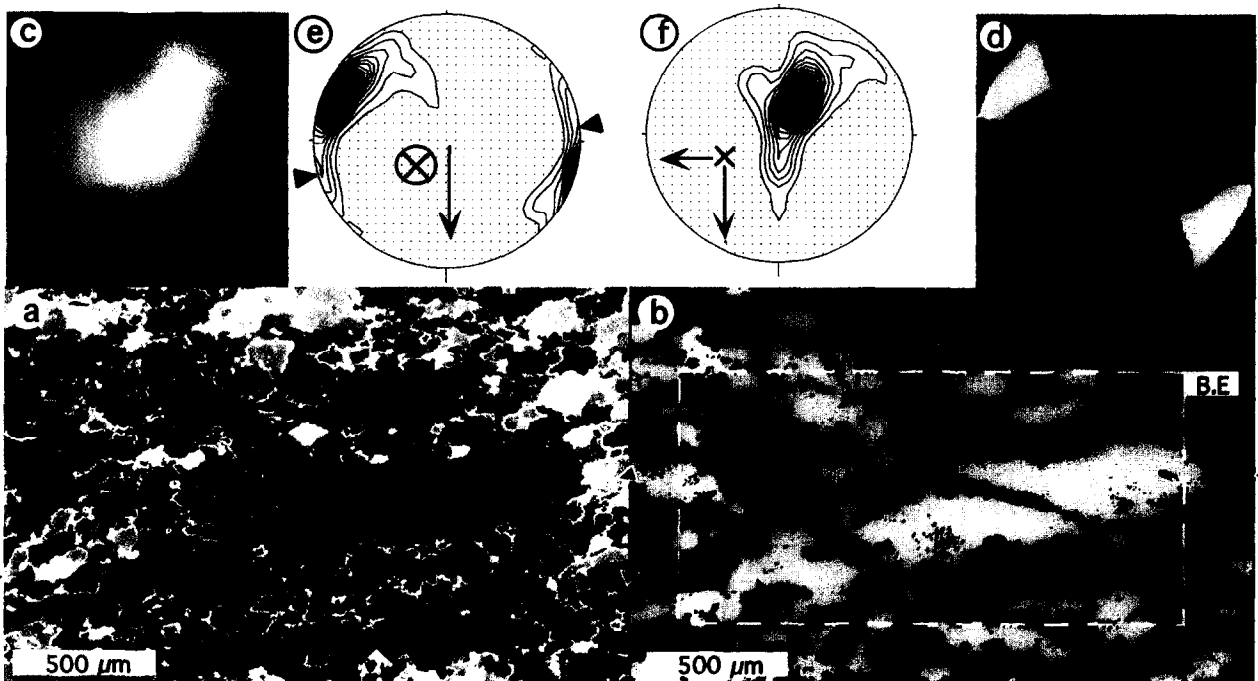

Fig. 9. CIP analysis of domain B.E. Domain boundaries are marked by dashed rectangle. See Fig. 2(b) for location in specimen. Arrows indicate that foliation is inclined with respect to horizontal. (a) Orientation image using standard CLUT (c) (see text). (b) Orientation image using problem adapted CLUT (d). (c) Standard colour look-up table (CLUT). (d) Problem adapted CLUT (for definition, see Fig. 4b). (e) Volume weighted stereogram of domain B.E. (f) Same as (e) rotated into plane of section A.
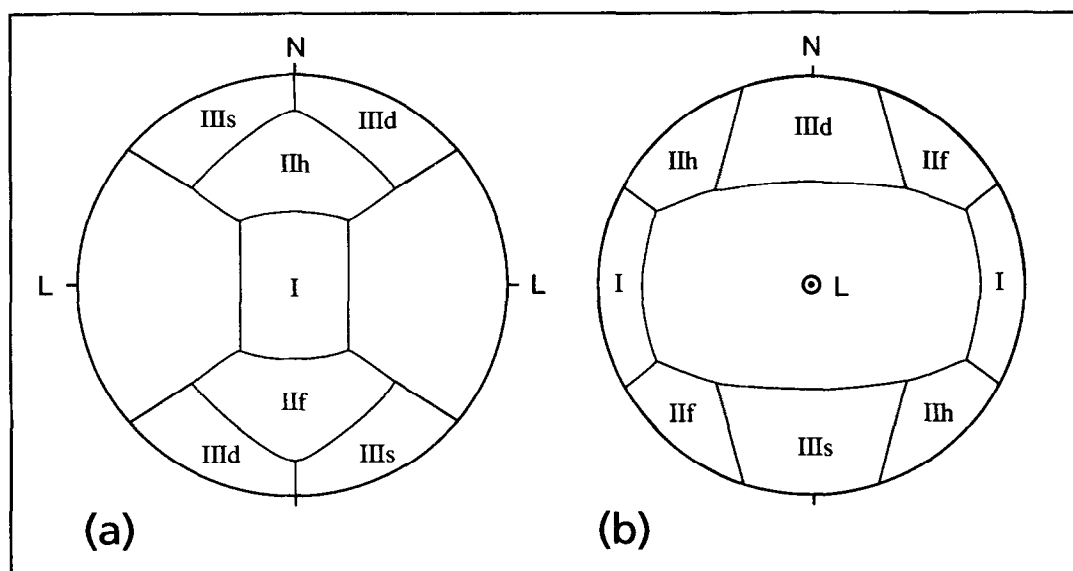
Fig. 4. Definition of c-axis direction groups (L lineation, N normal to foliation); upper hemisphere projection. (a) Pole figure parallel to section A. (b) Pole figure parallel to section B.

because they represent additional potential slip planes. The a-axes play an absolute key role since they represent the dominant slip direction in quartz (Bouchez 1978).

In general, the area measured by the texture goniometer depends on the 2 theta angle, the amount of tilting of the sample and the focus (i.e. the spot size) of the X-ray beam. These parameters vary during the measurement. As a consequence, the outlines of the measured areas depicted in Figs. 2(a,b) and Figs. 3(a,b) are not exact.

Bulk textures

Bulk textures obtained from two scans oriented perpendicular to the trace of the foliation are presented in Fig. 5(a–h). The areas scanned in the A- and B-section are indicated in Fig. 2 (areas A.s and B.s). For ease of comparison the results are presented twice: once in a plane parallel to the lineation (Fig. 5a & c), and once normal to the lineation (Fig. 5b & d).

The pole figures derived from the mutually perpendicular sections are remarkably similar confirming that they do indeed represent the bulk texture of the specimen. There are slight differences however in the location of the c-axis maxima. In section A.s, they occupy the IIh and IIf direction groups, while in section B.s, one of the two maxima falls into direction group I. A high density ridge connects the maxima and is oriented perpendicular to the lineation.

The IIId maximum is at a higher angle to the foliation normal than the IIIs maximum. This slight asymmetry of the c-axis 'fabric skeleton' indicates a sinistral sense of shear (Lister *et al.* 1978, Lister & Williams 1979) as expected from the regional context.

Positions and contours of high-density areas of a and m, contained in the basal plane (indicated by black triangles in Fig. 5b & d), are largely determined by the position of the two c-axis maxima. To a first approxima-
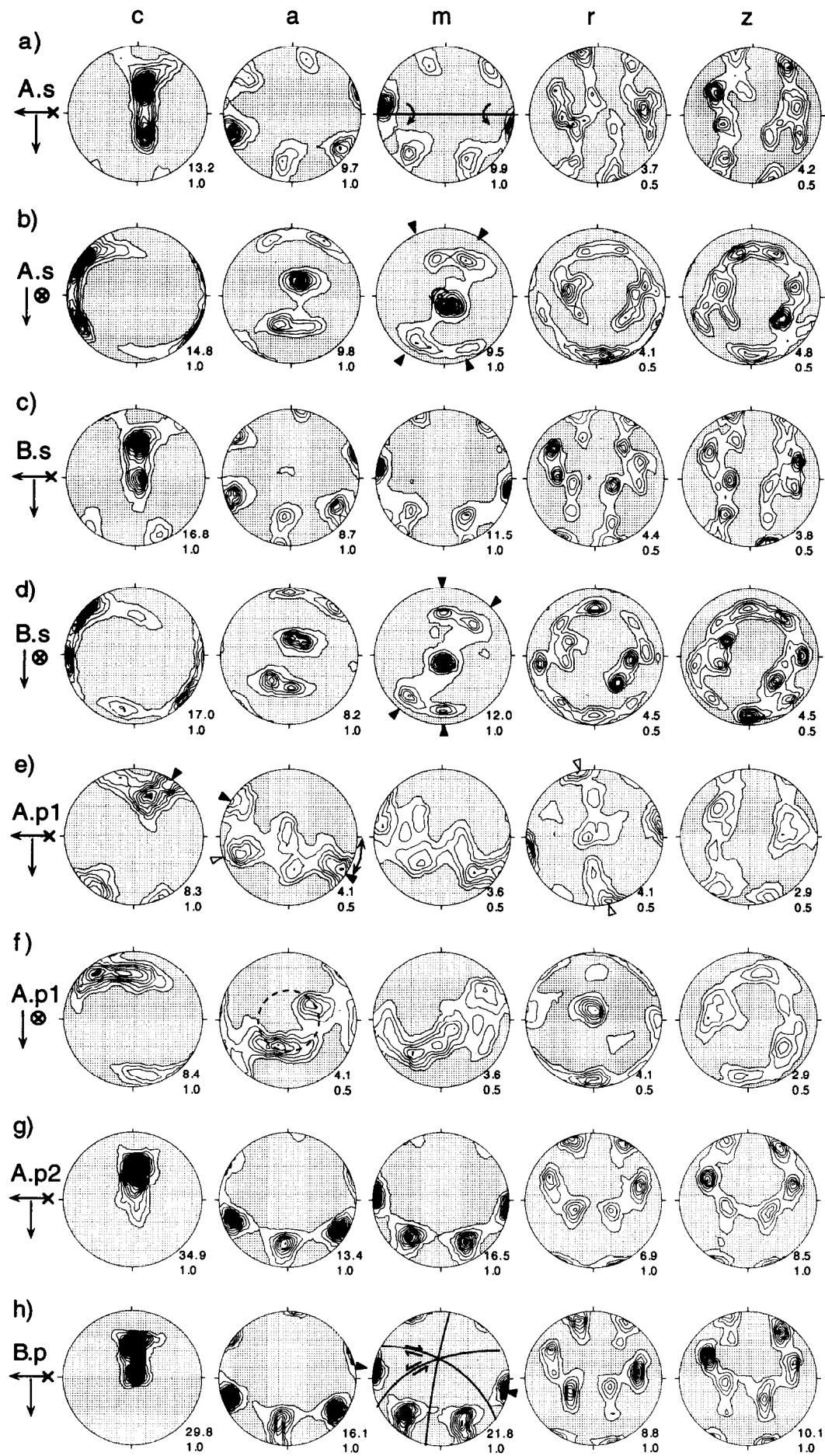
tion the bulk texture corresponds to two single crystal orientations. While the basal planes of the two preferred single crystal orientations intersect along a direction parallel to the lineation, they do not share a common a- or m-direction, as is frequently found for single and crossed girdle textures (Schmid & Casey 1986). The pole figures for r and z (positive and negative rhombs), however, indicate that there is little discrimination between positive and negative forms. This 'hexagonal' character indicates that basal or prism slip is more likely to have been active, since slip on r and z leads to a separation of positive and negative forms, and hence to a 'trigonal' character of the texture (Schmid & Casey 1986).

All maxima of the pole figures of Fig. 5(b) and (d), are more or less elongated along small circles around the lineation. The amount of elongation of the contours and strength of the a- and m-maxima are a function of the angle between the maxima and the axis of rotation (marked on the m-pole figures of Fig. 5a & b). Interestingly, the axis of rotation is parallel to the lineation but not to any of the rational crystal directions such as a or m. At the same time it is contained within the basal planes of the two preferred c-axis orientations. This observation will be crucial when interpreting the observations made with the CIP method.

Domainal textures

The pole figures obtained from the measurements taken with a scanning direction parallel to the trace of the foliation are shown in Fig. 5(e–h). Scan A.p1 exclusively samples fully recrystallized domains while area A.p2 includes a ribbon grain (see Figs. 2a and 3a). The third scan, B.p (see Figs. 2b & 3b), includes ribbon grains and some clast fragments.

The c-axis maximum from scans A.p2 and B.p (Fig. 5g and h) is again elongated in the plane perpendicular to the

Figure showing pole figures arranged in rows a) through h) and columns c, a, m, r, z.

a) A.s — c 13.2/1.0, a 9.7/1.0, m 9.9/1.0, r 3.7/0.5, z 4.2/0.5

b) A.s — c 14.8/1.0, a 9.8/1.0, m 9.5/1.0, r 4.1/0.5, z 4.8/0.5

c) B.s — c 16.8/1.0, a 8.7/1.0, m 11.5/1.0, r 4.4/0.5, z 3.8/0.5

d) B.s — c 17.0/1.0, a 8.2/1.0, m 12.0/1.0, r 4.5/0.5, z 4.5/0.5

e) A.p1 — c 8.3/1.0, a 4.1/0.5, m 3.6/0.5, r 4.1/0.5, z 2.9/0.5

f) A.p1 — c 8.4/1.0, a 4.1/0.5, m 3.6/0.5, r 4.1/0.5, z 2.9/0.5

g) A.p2 — c 34.9/1.0, a 13.4/1.0, m 16.5/1.0, r 6.9/1.0, z 8.5/1.0

h) B.p — c 29.8/1.0, a 16.1/1.0, m 21.8/1.0, r 8.8/1.0, z 10.1/1.0

lineation, as observed for the bulk texture above. This demonstrates that the major features of the bulk textures are controlled by single crystal domains such as ribbons and clasts.

A significantly different texture is found in the recrystallized domain A.p1 (Fig. 5e & f). Since it is considerably weaker it adds only little to the bulk texture. The c-axis maxima fall into direction groups IIIs, IIId and IIIh. The a- and m-maxima are more evenly dispersed within the basal plane than in the case of the other textures that are dominated by ribbon and clast domains. Also, the dominant a-maximum lies within the primitive circle of the pole figure for the A section (Fig. 5e, triangles). Viewed in the B-section (Fig. 5f) the a-axis maxima have a tendency to form small circles around the lineation. The r- and z-pole figures indicate that this texture has a 'trigonal' character.

The constrictional strain inferred from the shapes of ribbons and clasts is confirmed by the small circle a-axis distribution around the stretching lineation (compare Bouchez 1978, Schmid & Casey 1986, their sample SE 85). The asymmetry of the c- and a-pole figures, as seen in the A section of Fig. 5(e) is interpreted in terms of dextral shear, in contrast to the sinistral sense of shear inferred for the bulk texture and from regional studies. In view of the strain partitioning between different domains and given the departure from simple shear, such reversals in sense of shear within the same specimen are tolerable.

The texture (Fig. 5e) is a 'classical' one, indicating the simultaneous operation of basal slip and slip on the rhombs, or alternatively, slip on the steep rhombs π (see Schmid & Casey 1986, Law et al. 1990). However the microstructure within the scanned domain A.p1 (Figs. 2a and 3c) clearly reveals the existence of fabric domains on a smaller scale, each characterized by a different c-axis direction group. Hence, the c-axis pole figures of A.p1 represent a composite of the three dominating direction groups IIh, IIIs and IIId. Grains belonging to direction group IIh give rise to two a-axis maxima located off the trace of the basal plane and corresponding to direction group IIId, marked by full triangles in the a-axis pole figure of Fig. 5(e). Slip parallel to the leftmost of these a-maxima (indicated by a open triangle on the a-axis pole figure in Fig. 5e) is interpreted to have used r-planes, the poles of which are marked by open triangles on the r-pole figure in Fig. 5(e). Thus, within the optical domains characterized by the IIh direction group, the obliquity of the inferred slip on r indicates a sinistral sense of shear.

C-axis positions in direction groups IIIs and IIId indicate suitable orientations of basal planes for sinistral and dextral slip, respectively. For example, grains of c-

axis direction group IIId correspond to a prominent a-axis maximum, disposed at roughly 30° to the foliation and the lineation (see full triangles in Fig. 5e).

DOMAIN CHARACTERIZATION WITH CIP

For an extensive review of the CIP method, the reader is referred to Panozzo Heilbronner & Pauli (1994); the details of the MacCIP implementation are described in Pauli (1995). The method is based on image processing techniques (Panozzo Heilbronner & Pauli 1993, 1994) and allows the calculation of absolute orientation of the c-axis at each pixel. These pixels are then coloured according to a colour look up table (CLUT), which may be viewed as a coloured stereogram.

Orientational resolution of azimuth and inclination is 1°. By counting the number of pixels per orientation, volume-weighted stereograms may be obtained. By selecting the appropriate region within the image, the stereogram of an individual domain is obtained. Such stereograms were calculated and contoured with an extended version of Stereoplot by N. Mancktelow (1993). The contouring of CIP-derived pole figures is in multiples of the uniform distribution. Regions above the eighth contour are filled black and referred to as maxima.

Using CIP derived orientation images, the segmentation into fabric domains can be performed much more precisely than by a hand drawing on an ordinary photomicrograph. Here, domains were separated according to the homogeneity of the texture pattern. Figure 6 summarizes the domain types as derived by the CIP method from sections A and B.

Orientation images taken from differently oriented thin sections can be compared directly by rotating the CLUT about the appropriate angle. Identical c-axis orientations will then have identical colours. An example of this is portrayed in Figs. 8 and 9. Rotation of the CLUT pertaining to section A (Fig. 8d) into the orientation of section B yields the CLUT shown in Fig. 9(d) and permits the comparison of the absolute c-axis orientations of section A and B.

CLASTS

The large lenticular augen-shaped clast seen in hand specimen is also visible in thin section B (see Figs. 3b and 7). The c-axes of the clast as well as those of the entire area B.p (of which it is a part) are closely parallel to the section plane, as evidenced by the peripheral arrange-

Fig. 5. Pole figures measured by X-ray goniometry and calculated from the ODF. Location and size of scanned areas are indicated in Fig. 2. Pole figures (upper hemisphere) are contoured in multiples of a uniform distribution (m.u.d.). Maximum intensity and contour interval are shown at the lower right of each pole figure. Intensities above 8 m.u.d. are black; intensities below 1 m.u.d. are stippled. For arrows and triangles, see text. (a–d) bulk textures, (e–h) domainal textures. (a) Scan A.s, as measured, lineation E–W. (b) Scan A.s, rotated, lineation in the centre. (c) Scan Bs, rotated, lineation E–W. (d) Scan B.s, as measured, lineation in the centre. (e) Scan A.p1, as measured, lineation E–W. (f) Scan A.p1, rotated, lineation in the centre. (g) Scan A.p2, as measured, lineation E–W. (h) Scan B.p, rotated. lineation E–W.

ment of c-axes in the stereogram (inset in Fig. 7). Assuming a constant inclination of 0° for the clast, the azimuths of the c-axes were traced. The range of c-axis orientations thus obtained spans at least 60° in a plane normal to the lineation (oriented perpendicular to the sketch of Fig. 7).

The variation of c-axis orientations within the clast is not gradual. Instead, it occurs abruptly at the boundaries of the c-axis-parallel fan shaped deformation bands. On the right, the quartz clast is broken along steeply oriented fractures (arrows in Fig. 7). The fractures are filled with recrystallized quartz grains. This fracturing occurred late during the deformation history, because the outlines of the deformation bands and the c-axis orientations can be correlated across the fractures.

The areas analysed by texture goniometry (B.s and B.p) include parts of the clast depicted in Fig. 7. The recalculated c-axis pole figure of the area B.p (Fig. 5h)

was rotated and used as an inset in Fig. 7. For later discussions, the X-ray goniometry results obtained for area B.p will be used as representative for the clast too. Here, we note that the spread of the c-axes is in a plane normal to the lineation. This feature is interpreted to indicate basal slip in a direction perpendicular to the lineation. Thus, the lineation becomes the axis of external rotation responsible for the fanning of the c-axes.

RIBBON GRAINS

In section A (e.g. Fig. 2a) non-recrystallized and strongly elongated quartz ribbons appear as 'rubans monocrystallins' (see discussion by Boullier & Bouchez 1978). In section B (e.g. Fig. 2b) they appear as lenticular domains. The summary in Fig. 6 shows that the c-axis

Ribbon grains

Direction group		SPO	α
A.I			40°
A.G			20°
B.E			-

Monomaximal recrystallized domains

Direction group		SPO	α
A.A			150° 45°
A.B			35°
A.E			
A.H			
B.A			
B.C			15°

Polymaximal recrystallized domains

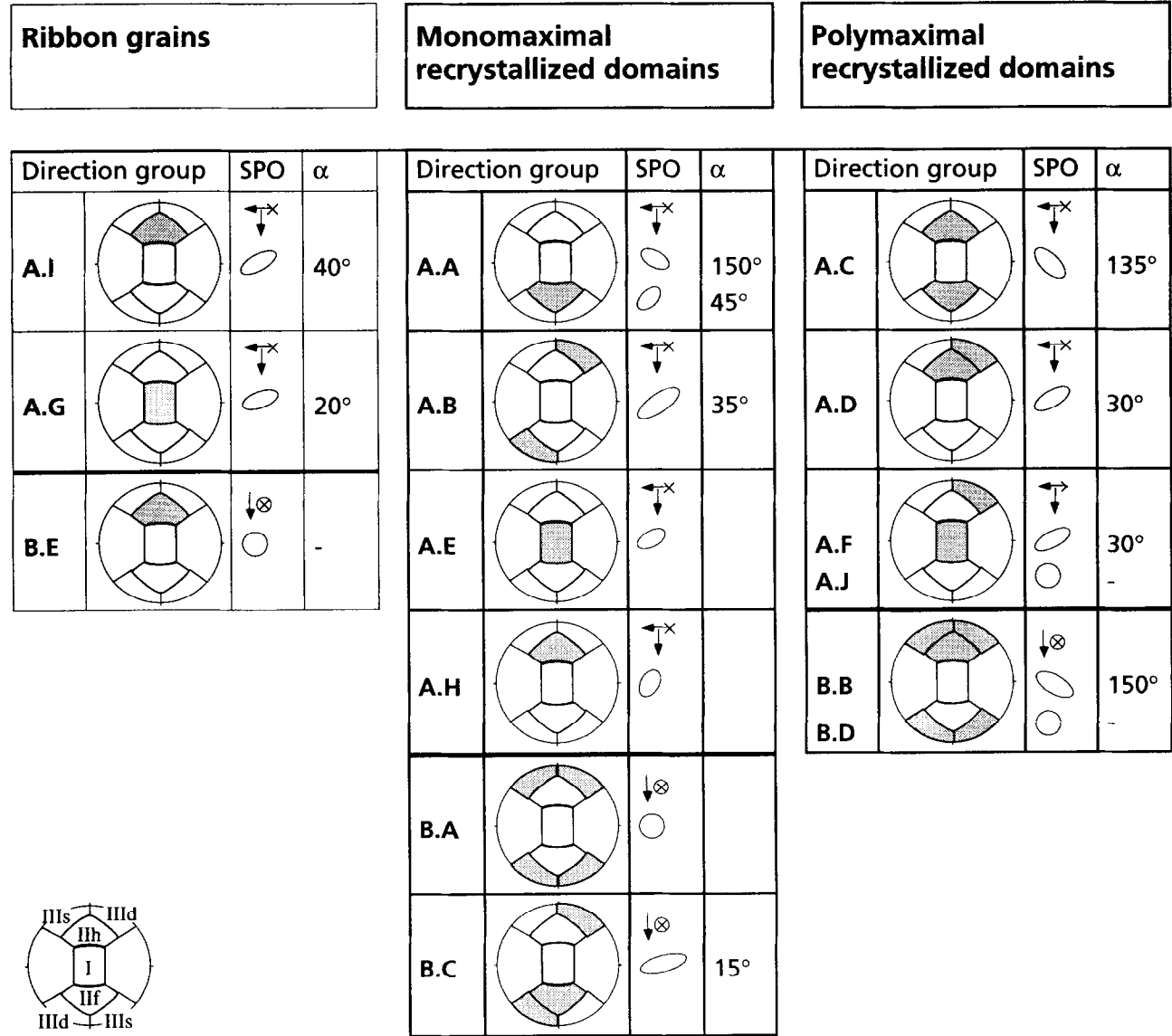| Direction group		SPO	α
A.C			135°
A.D			30°
A.F A.J			30° -
B.B B.D			150° -

Fig. 6. Summary table of shape and fabric analyses of mono- and polymaximal domains. First column: name of domain; second column: stereogram of direction groups occupied by domain (lineation E–W), third and fourth column: characteristic shape and angle anti-clockwise with respect to horizontal (see text for further discussion).
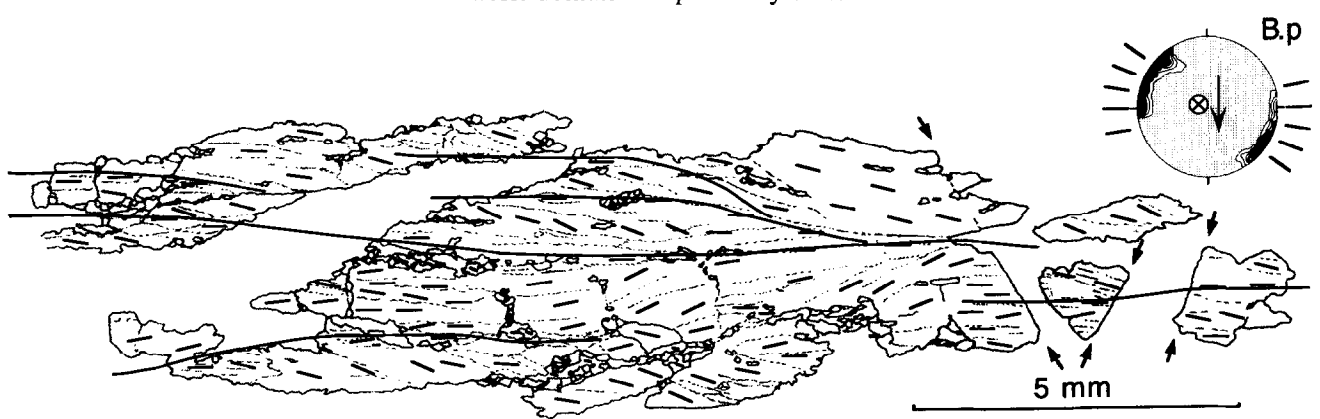
Fig. 7. Line drawing of distorted and kinked quartz clast of section B. Stippled lines are subgrain and deformation band boundaries. Heavy lines indicate strike of the c-axis. Regions of horizontal c-axis orientations are connected with heavy lines. Upper right: c-axis pole figure derived by X-ray texture goniometry from scan B.p inserted for comparison. The range of orientation of c-axes of the clast is marked at periphery.

orientations of ribbon grains fall into the direction groups IIh and I.

Figure 8 shows orientation images, calculated in the central part of section A, crossing a strongly undulous ribbon grain denoted as domain A.I. Colouring with the standard CLUT (Fig. 8c) beautifully displays the undulous extinction (Fig. 8a). The problem-adapted CLUT (Fig. 8d) is subdivided following the direction groups defined in Fig. 4. The resulting orientation image (Fig. 8b) shows less orientational detail. Instead it reveals that most of the grains of the image fall in direction group I (red) and IIh (yellow). More detail is shown in the c-axis pole figure of the ribbon grain (= domain A.I) which is dominated by the IIh maximum (Fig. 8f). The same is found in the X-ray texture (Fig. 5g) obtained for area A.p2 (Fig. 2a) which includes the area considered here.

Remembering that the elongation of the c-axis maximum is due to a rotation about the lineation direction, we may now see this as the change of blue shades in the orientation image of Fig. 8(a). The ribbon domain boundary is irregular and controlled by the shape of the recrystallized grains in the neighbouring domains (Fig. 8a). The local grain boundary orientation is inclined by 20° to 45° (typically 40°) with respect to the foliation (Fig. 6).

Figure 9 shows the orientation images of a lense-shaped ribbon grain (domain B.E) from section B. Orientation details are best seen in Fig. 9(a) where a standard CLUT (Fig. 9c) was used. The c-axes (Fig. 9e & f) belong to the direction group IIh, similar to the ribbon grain in section A. On the basis of c-axis orientation alone, it is difficult to distinguish between ribbon grain and recrystallized grains (compare Figs. 8b and 9b). Moreover, the variation of c-axis orientation between the surrounding recrystallized grains and the ribbon grain is comparable to the spread within the ribbon grain.

A third ribbon grain, domain A.G, was analysed in section A (Fig. 10). The c-axis maximum of this domain is in direction group I, i.e. perpendicular to lineation and within the foliation. This is an ideal orientation for prism slip, responsible for the elongation of the ribbon grains parallel to the lineation.

The local orientation of the domain boundaries was analysed with the SURFOR method (Panozzo 1983); the results are presented in Fig. 11(c). In contrast to the local orientation mentioned so far, the global orientation of the domain boundaries is parallel to the foliation. In section A, the local domain boundary orientation is not symmetric with respect to the foliation; instead, it is inclined by 15–20°. In contrast, on section B, such an asymmetry cannot be detected (Fig. 11c).

In combination, the observations made on sections A and B support the notion of a rod- or cigar-shape of the ribbon grains in this sample. The ribbon domain surfaces exhibit complex geometries on the scale of the surrounding recrystallized grains (approximately 100 μm). The symmetric and asymmetric bulges of the ribbon boundaries in sections B and A, respectively, are the traces of an asymmetrically napped surface in three dimensions. Asymmetric bulges along grain boundaries are known as a microstructural shear criterion and probably reflect the local sense of gliding along grain boundaries (Drury & Humphreys 1988). Hence, the asymmetry of the boundaries of domain A.G (Fig. 12) is taken to indicate a dextral sense of shear along the ribbon grain boundary, i.e. again opposite to the regional sense of shear in the Corvatsch mylonite zone.

One may argue that five domain boundaries on section A and three on B are not sufficient to infer bulk shear sense. In fact, on section A, most domains adjacent to the analysed boundary surfaces are composed of grains with 'dextral' shape preferred orientation; on section B, a 'dextral' and a 'sinistral' domain are present. Since the symmetry or asymmetry of domain boundaries depends on the shape of the recrystallized grains adjacent to them, the apparent 'overall' asymmetry of section A and the symmetry of section B may be fortuitous.

MONOMAXIMAL RECRYSTALLIZED DOMAINS

Monomaximal domains consist of recrystallized grains which have a clear maximum in one single direction (Fig. 6).
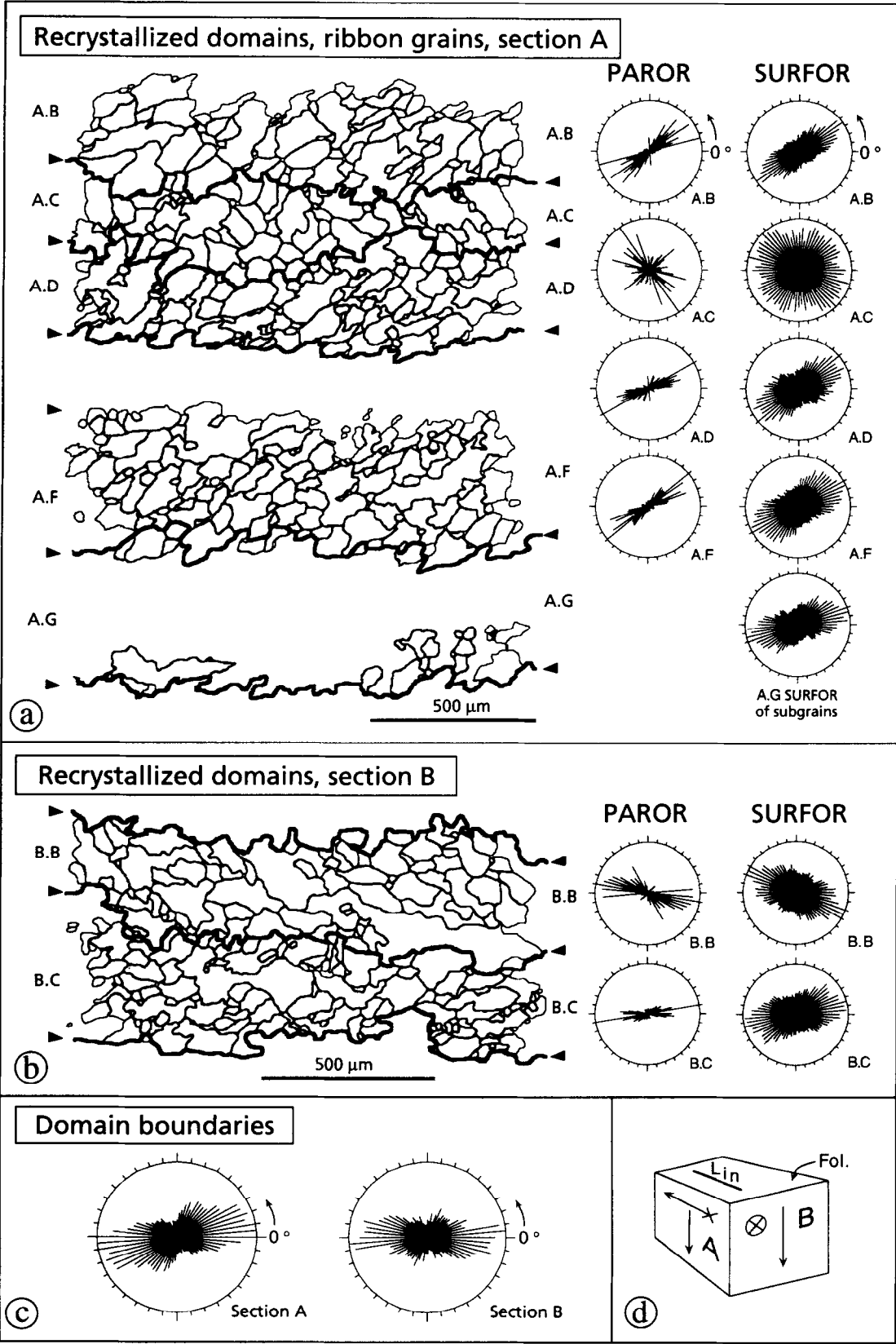
Fig. 11. (a) Shape analyses of selected domains from section A. Number of particles is 88 for A.B, 86 for A.C, 117 for A.D, 157 for A.F and 25 for A.G. The preferred orientations of the grain boundary surface (SURFOR) and of the long axes of grains (PAROR) are shown in the rose diagrams (see text for discussion). (b) Shape analysis of selected domains B.B and B.C of section B (perpendicular to the lineation). For the location of domains, see Fig. 2. The preferred orientation of the grain surfaces (SURFOR) and the grain long axes (PAROR) show opposite dispositions. See text for discussion. (c) Preferred orientation (SURFOR) of domain boundaries. (d) Sample reference frame.
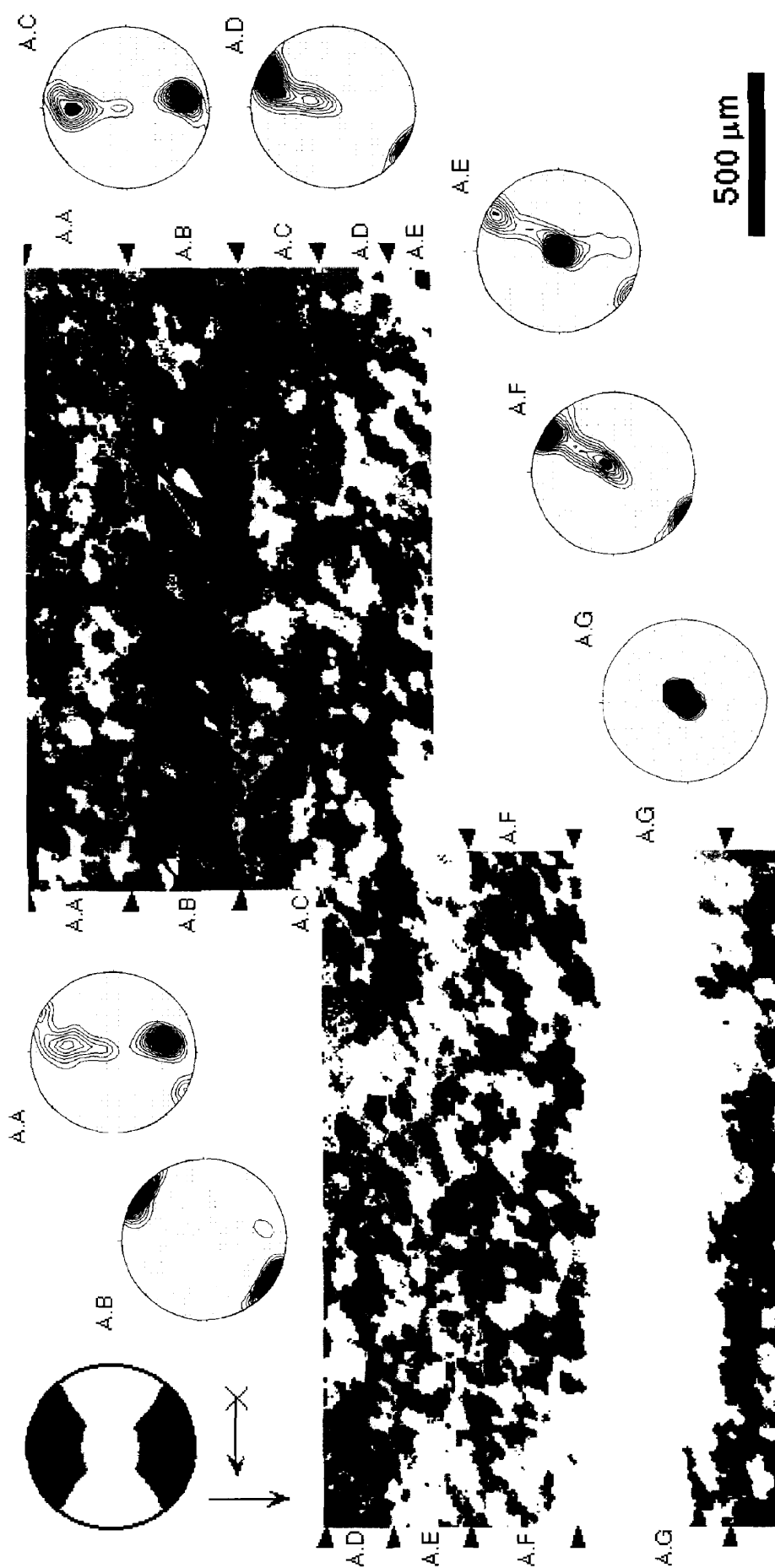
Fig. 10. CIP analysis of domains A.A to A.G of thin section A (see Fig. 2a for location). Orientation images using problem adapted CLUT and CIP derived c-axis stereograms. Domain boundaries are indicated by triangles. Arrow in domain A.B is parallel to the SPO of the grain surfaces and the bulges of the domain boundary.
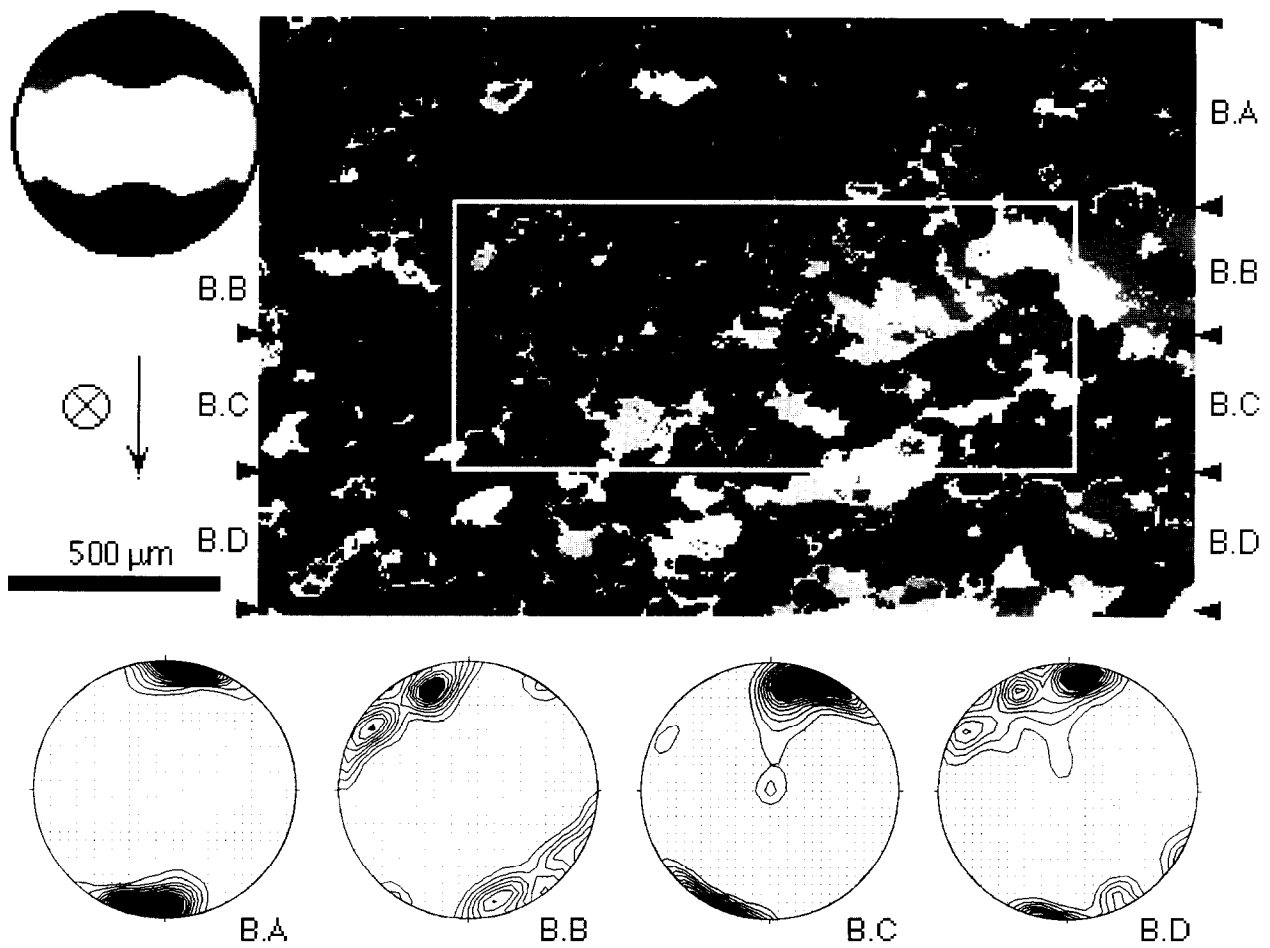
Fig. 12. Orientation image and c-axis pole figures of four domains of section B (see Fig. 2b for location). Domain boundaries are indicated by triangles. Rectangle shows location of shape analysis of Fig. 11(b).

IIId-domains

The most spectacular monomaximal recrystallized domains are the domains belonging to direction group IIId as for example domain A.B (Fig. 10). This domain consists of recrystallized, elongated grains (see Fig. 3c); the grain boundaries as well as the particle long axes are preferentially aligned with an angle of 35° to the foliation (Fig. 11a, white arrow on Fig. 10).

Pole figures derived by X-ray goniometry of A.p1 (Fig. 5e & f) include the domain A.B and thus add insight to the domainal texture of the IIId direction group. The c- and a-axes maxima that are typical for domains with direction group IIId are marked by triangles along the periphery of the pole figure in Fig. 5(e).* The a-axes at the periphery of this figure are rotated by approximately 30° (clockwise) with respect to the lineation. This places them in a conjugate orientation of 65° with respect to the preferred grain and grain boundary alignment (see Fig. 11).

I-domains

Domain A.E (Fig. 10) predominantly consists of a trail of grains belonging to direction group I. The grains show a large variability in grain size and grain shape. Such microstructural features are typical for the tips of domains which are seen to pinch out gradually in the direction of the lineation within the section A. This kind of recrystallized domain is interpreted as the relict of former ribbon grains. Note that the ribbon domain A.G nearby also falls into direction group I (Fig. 10).

IIIs and IIIs/d domains

Figure 12 illustrates monomaximal recrystallized domains which either belong to direction group IIIs (B.C) or which fall between IIIs and IIId (B.A). The lenticular domains are approximately 500 μm thick and 10 mm wide. Shape analysis was performed on an area where domain B.B pinches out laterally (see Figs. 2b and 3b). The grain boundaries and particle long axes are inclined with respect to the foliation plane, but with a different sense of obliquity for domains B.B and B.C (herringbone microstructure; Fig. 11b).

The IIIs/d direction group is characterized by a speckled appearance in the orientation images (in particular domain B.A in Fig. 12), which is due to the definition of the direction group whose limits crosscut the maximum of the c-axis orientation. Grains in this domain do not show a marked shape preferred orientation.

Domain and grain boundaries of recrystallized monomaximal domains

In as much as different domains may deform at different rates, domain boundaries may be the sites where strain incompatibilities between the domains are accommodated. The component of the migration that is oriented perpendicular to the domain boundary gives rise to growth or collapse of the domain. If both domain boundaries migrate in the same direction, the grain configuration of the domain may migrate as an entity through the material (comparable to the fast grain boundary migration of single grains in the high T analogue experiments of Means 1983). Since all domains of section A are of similar size and shape, 'domain boundary migration', which would lead to the growth of some domains at the expense of others, is excluded. Instead we interpret domain bulging to be strain induced and caused by compatibility requirements between the domains. This confines bulging to the domain boundary region. Bulging may be associated with domain boundary-parallel sliding along grain boundaries, as proposed by Drury & Humphreys (1988). If so, this would indicate grain boundary sliding concentrated along the domain boundary (compare e.g. Lister & Snoke 1984, fig. 14, Drury & Humphreys 1988).

The asymmetric inclination of grain boundaries of recrystallized grains within the domains is often taken as, an indicator for the sense of shear (e.g. Simpson & Schmid 1983, fig. 10, Lister & Snoke 1984). Since the sense of obliquity changes from domain to domain in both sections A and B (Fig. 11) the net sense of shear is difficult to determine.

In general, the preferred grain boundary alignment and the long axes of recrystallized grains in sections A and B have a tendency to be at a relatively small angle to the c-axis orientation (e.g. domain A.B in Fig. 10), confirming the findings of Garcia Celma (1982). The elongation of quartz grains parallel to the c-axis coincides with a high diffusion anisotropy parallel to the c-axis (Linker & Kirby 1981, 1984, Mainprice & Nicolas 1989). The resulting creep anisotropy of single quartz crystals may influence grain boundary migration and thus the shape of grains. Alternatively, elongated grains may be generated from deformation bands. These are often formed subparallel to the c-axis and may evolve into grain boundaries during continued deformation, thereby promoting an elongated shape of the newly forming grains (see discussion below).

POLYMAXIMAL RECRYSTALLIZED DOMAINS

Polymaximal domains, characterized by two or more dominant direction groups (overview in Fig. 6) have bulk shapes (layers in section A, lenticular in section B) and sizes identical to those of monomaximal domains.

IIh + IIf domains

Domain A.C exhibits a c-axis pole figure composed of two prominent maxima in direction groups IIh and IIf (Fig. 10). The obliquity of long axes of grains is of opposite sense with respect to that of the grains of domains A.B and A.D (Fig. 11). This herringbone microstructure (Garcia Celma 1982) is also associated with alternating c-axis orientations (Fig. 10).

I + IIId domains

Domains A.F (Fig. 10) and A.J (Fig. 8g) are composed of grains belonging to direction groups I and IIId. The type of *c*-axis pole figure characteristic of these domains is found quite often (e.g. Knipe & Law 1987, Fueten *et al.* 1991). Domain A.F shows elongated grain shapes and preferred grain boundary alignment oblique to the domain boundary (Fig. 11a), indicating a dextral sense of shear.

II + IIIs/d domains

Domain B.B is dominated by direction group IIIs (when viewed in a plane parallel to section B, Fig. 12). It again illustrates the herringbone microstructure of recrystallized domains. The dimensional preferred orientation in domain B.B is opposite in sense to that found in the monomaximal domain B.C (Fig. 11b) correlating with the opposite sense of obliquity of the *c*-axis pole figures. The sinistrally oblique dimensional orientation of the grains in domain B.B dominates the central part of section B. Shearing in section B, i.e. in a plane perpendicular to the lineation, draws attention to the three-dimensional nature of strain partitioning in this specimen.

INTERPRETATION OF FABRIC DOMAIN EVOLUTION

The previous descriptions strongly suggest that the sample has not been deformed under plane strain conditions, the pronounced fabric heterogeneity indicating that strain is extremely heterogeneous. Hence, individual domains are not expected to have been deformed according to the strain path of the bulk specimen imposed by the overall movement along the Corvatsch mylonite zone.

The initial grain size may be estimated from the size of clasts and ribbon grains. The clast preserved in the lower half of section B (Figs. 2b and 7) indicates a grain diameter well in excess of 10 mm at least for some of the original grains. In contrast, ribbon grains are prolate with typical dimensions of 20 mm × 2 mm × 0.6 mm, oriented parallel to the lineation. This corresponds to a diameter of less than 3 mm for the initially spherical grain. Unless we allow for a relatively high dispersion of the initial grain size distribution, one may infer that during the first stages of deformation the originally larger grain size was comminuted by fracturing and/or recrystallization (see Lloyd *et al.* 1992). Since domain grain boundary migration was quite restricted (see previous discussions) the ribbon grains are inferred to have persisted as passive markers up to very large strains. This explains the domainal nature as an inherited feature and precludes the formation of a non-domainal fabric, as is occasionally found in the centre of shear zones formed within quartz veins (see Lloyd *et al.* 1992 and Law *et al.* 1990 for an

investigation of domainal and non-domainal fabrics in the same shear zone).

The earliest preserved stage of deformation is documented in the lenticular augen-shaped clast mentioned above (Figs. 2b and 7). This latter indicates moderate shortening perpendicular to the foliation plane. Subsequent deformation partitioning left the clast's fabric (texture and microstructure) unaltered while penetrative deformation affected the surrounding domains.

Basal and prism slip in clasts and ribbons during deformation

The texture measured by X-ray goniometry preferentially reflects the crystal orientations of large single crystal domains (clasts and ribbons). For inferring the active slip systems we apply the concept of the axis of external rotation (common crystal direction of both kinked and unkinked domains in a single crystal, see Turner & Weiss 1963). The axis of external rotation is contained within the active slip system and oriented perpendicular to the slip direction.

The axis of external rotation of the ribbons grains and clasts (marked on the *m*-pole figures in Fig. 5a & b) is parallel to the lineation and contained within the basal plane. The fact that the prominent slip direction in quartz is not perpendicular to *a* is explained by assuming that basal slip is the active slip system. Due to the simultaneous activity parallel to more than one *a*-direction, basal slip can have a net slip direction parallel to any direction within the slip plane. Here, it acts perpendicular to the lineation (S_b in Fig. 13a), leading to strain in the section B. The net slip vector S_b may be the result of combined slip along the two *a*-maxima situated near the lineation (see *a*-pole figure in Fig. 5h), or alternatively, predominant slip along the weakest, streaked out *a*-maximum at a high angle to the lineation and near S_b. The model depicted in Fig. 13(a) favours the first possibility, since combined activity along the two stronger *a*-axis maxima also permits components of slip parallel to the lineation direction.

Deformation in the B-section flattened the clast up to an aspect ratio of roughly 1:3. Subsequently, the clast broke along steeply oriented fractures (Figs. 2b,d and 7). The fractures, which postdate the fabric of the clast (see previous discussion), cannot be followed into the adjacent recrystallized quartz matrix, i.e. they do form while plastic deformation of the more ductile (due to recrystallization) domains around the clast continued.

While basal slip accommodated flattening in a plane parallel to section B it cannot produce a net elongation parallel to the lineation because material lines contained within the slip planes cannot be stretched. Basal slip in ribbon grains that fall into direction group I, such as domain A.G (Fig. 10), cannot achieve any deformation depicted parallel to section A. Hence, other slip systems must be invoked for the substantial elongation of the ribbons parallel to the lineation. The 'hexagonal' character of the texture discussed earlier reduces the choice to prism and/or basal slip. Prism slip can simultaneously
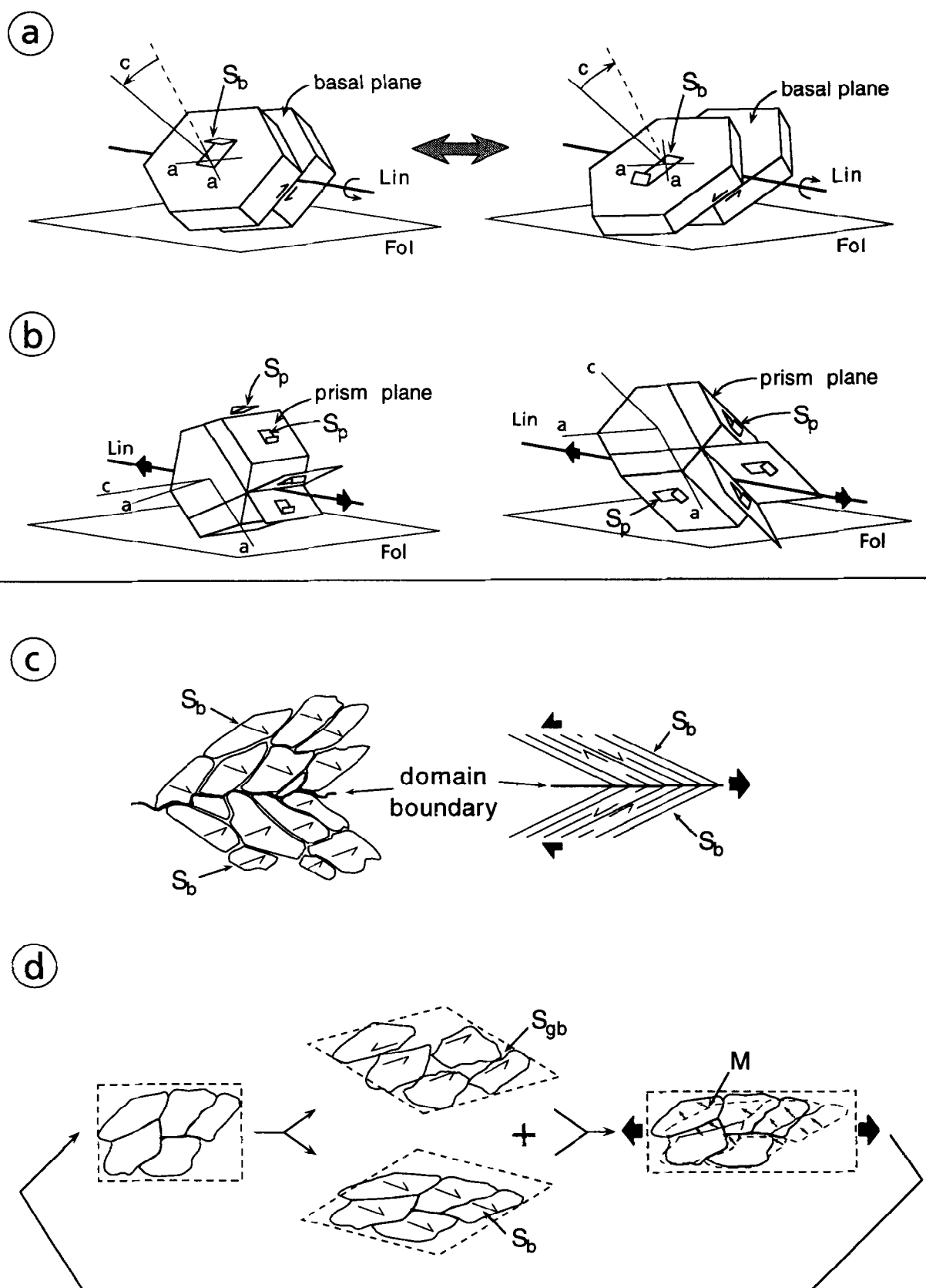
Fig. 13. Kinematic models of c-axis orientation of domains. See text for discussion. (a) Rotation of c-axes by combined slip along two a-axes in the basal planes (resulting slip vectors S_b). (b) Elongation (heavy arrows parallel lineation) domains by combined slip along two a-axes in the prism planes (slip vectors Sp). (c) Bulk elongation (heavy arrows) by slip along the inclined basal planes (fine S_b arrows). (d) Elongation of individual domain (heavy arrows) by a combination of intracrystalline slip along basal planes (fine S_b arrows) and intercrystalline slip on microshears along inclined grain boundaries (S_{gb}). Dashed boxes schematically indicate domain shape changes.

operate along two prism planes and parallel to two *a*-maxima situated near the primitive circle of the pole figure and near the lineation in the A section (as marked on the *m*-pole figure in Fig. 5h and sketched in Fig. 13b left). The operation of these two prism planes in a conjugate sense achieves the stretch parallel to the lineation.

In summary, we conclude that both basal and prism slip accommodate the constrictional strain indicated by the ribbon and clast grains. Basal slip is responsible for shape changes parallel to the B section while prism slip produces the simultaneous elongation parallel to the lineation. The single crystal character of the texture is not strain induced, but inherited from large original single crystals.

Later stages of deformation in the ribbon domains

The necking microstructure of one of the ribbon grains in section A (arrows in Figs. 2a and 3c) indicates a more competent behaviour of the ribbons with respect to the dynamically recrystallizing domains. This directly indicates a partitioning of the deformation in the sample between the ribbon domains and the recrystallized domains. Compatibility with the deformation of neighbouring recrystallized domains is ensured by small scale grain boundary migration along domain boundaries, as discussed earlier.

The trails of direction group I grains of the recrystallized domain A.E (light gray grains in Fig. 10) probably represent relics of a former ribbon grain which did eventually recrystallize. However, ribbon grains of direction group IIh (domain A.I in Fig. 8, and domain B.E in Fig. 9) have crystal orientations that accommodate the imposed strain without recrystallization particularly well. The crystal orientation of direction group IIh ribbon grains as derived with CIP and X-ray goniometry (e.g. Fig. 5g) shows the basal plane to be at an angle of roughly 45° to the foliation (sketched in Fig. 13b right). Such ribbon grains can be simultaneously stretched parallel to the lineation by prism slip and deformed within the B-planes by basal slip. The persistence of suitably oriented clasts points to selective dynamic recrystallization of those clasts and ribbon domains which are unsuitably oriented for achieving the imposed strain by intracrystalline slip (see discussion of a recent controversy regarding this issue in Schmid 1994).

Recrystallized domains: the last stages of deformation

The previous discussion showed that ribbon grains occasionally transform into recrystallized domains. This, together with the similar shapes and dimensions of ribbon and recrystallized domains, suggests that recrystallized domains do indeed evolve from individual large grains. During further straining they persist as separate entities, maintaining similar shapes and dimensions (see Lloyd *et al.* 1992 who arrived at similar conclusions).

We will first investigate the deformation mechanisms active in monomaximal domains dominated by *c*-axis orientations in direction group III, such as domain A.B (Fig. 10). Grains within this domain have their basal plane and a prominent peripheral *a*-axis maximum at an angle of roughly 30° to the foliation and lineation (indicated in Fig. 5e by full triangles). Basal slip is inferred to have been active, since none of the *m*-, *r*- or *z*-pole has a preferred orientation at 90° to this prominent *a*-direction (see Fig. 5e).

The model sketched in Fig. 13(c) (left) depicts the interaction between domains and is inspired by the herringbone microstructures of domains A.A, A.B, A.C and D.D (Figs. 10 and 11a). The neighbouring domains are dominated by IIId or IIIs *c*-axis direction group orientations having their basal planes (S_b in Fig. 13c) in a conjugate arrangement. Such a conjugate system is necessary to accommodate the bulk elongation of the sample parallel to the lineation (black arrows on Fig. 13c right). The basal planes that correspond to the *c*-axis orientations of the herringbone structures (Fig. 10) are not as systematically disposed about the foliation as sketched in Fig. 13(c). Nevertheless, this conjugate arrangement of domains can achieve substantial thinning in the A section. As discussed in the context of domainal X-ray textures, slip along an *a*-direction on conjugately oriented *r*-planes may also have been active. Hence Fig. 13(c) is a simplification of a more complex situation. However, numerical modelling of cells with one single slip system also produces domainal arrangements of conjugate slip systems (Gapais & Cobbold 1987).

The elongation of individual domains in a direction parallel to the lineation demands the operation of conjugate slip *within* the individual domains, and not segregated into neighbouring domains as proposed in Fig. 13(c). In Fig. 13(d) an alternative mechanism for the stretching of recrystallized domains is proposed. Within domains that are characterized by IIIs and IIId direction groups, synthetic intracrystalline slip again occurs in the direction of the prominent *a*-axis maximum along the inclined basal planes (S_b in Fig. 13d). Since prism $<c>$ slip is unlikely to have operated under low grade metamorphic conditions (Schmid *et al.* 1981, Schmid & Casey 1986) no other slip system can provide slip in a conjugate sense for this crystal orientation. Therefore, we suggest that the second, conjugate slip system is provided by antithetical microshears along the inclined grain boundaries (double arrow in Fig. 10, S_{gb} in Fig. 13c).

Conjugate slip along S_b and S_{gb} yields the desired finite domain elongation indicated by the heavy arrows in Fig. 13(d)(right). Slip along S_b and S_{gb} tends to rotate the grain boundaries (i.e. S_{gb}) towards the finite flattening plane. The observed high inclination of the grain boundaries with respect to the foliation is maintained by simultaneous grain boundary migration. The migration direction (M in Fig. 13d right) is opposite to the synthetic sense of intracrystalline slip in the quartz along the basal planes.

In summary, a combined activity of intracrystalline slip, strain induced grain boundary migration and grain boundary sliding is proposed to have accommodated the bulk shape change in domains dominated by the IIId and IIIs direction groups. The operation of intracrystalline slip and grain boundary sliding is also reported from higher grade quartzites (e.g. Behr 1961, Lister & Snoke 1984). Although rather speculative at this stage, the model proposed in Fig. 13(d) offers a possible explanation for the observed systematic dependence of the preferred grain boundary orientation sub-parallel to the c-axis.

Polymaximal recrystallized domains composed of IIh and IIf c-axis direction groups have enough potentially active slip planes. They have been evaluated with the help of the textures shown in Fig. 5 (a,b). It is assumed that the texture measured in ribbon grains is representative for recrystallized domains if the c-axis patterns are identical. The hexagonal symmetry of the bulk r- and z-pole figures in Fig. 5(a,b) suggests intracrystalline slip on basal and prism planes. As seen in the m-pole figure of Fig. 5(b) the traces of the basal planes are disposed at angles of 20°–30° to either side of the foliation plane normal (full triangles on Fig. 5b). Equating the a-axis maxima on either side of the lineation to the dominant slip directions on two steeply oriented basal planes and on inclined m-planes (see Fig. 13b right), a net stretch parallel to the lineation does result.

DISCUSSION AND CONCLUSIONS

Detailed three dimensional analysis of texture and microstructure of two mutually perpendicular sections across a specimen deformed by constrictional strain revealed an extremely domainal fabric which strongly depends on the initial fabric configuration. The fabric is modified during deformation and dynamic recrystallization, but retains initial fabric elements, most notably clast fragments and ribbon domains. This leads to an oblique crystallographic preferred orientation which is not related in a straightforward manner to the bulk kinematics of the specimen. Due to strain partitioning, the inferred senses of shear of different fabric domains may be opposed.

The obliquity of intracrystalline slip directions (a-axes) with respect to the lineation (the finite elongation direction) demands the activity of at least two slip systems for achieving a bulk lineation-parallel stretch. For grains falling into c-axis direction groups I and II, this stretch is achieved with two a-axes along conjugate prism planes, while basal slip is held responsible for shape changes in a section perpendicular to the lineation. Since the bulk deformation can easily be accommodated by intracrystalline slip planes, these grains form ribbon grains belonging to the c-axis direction groups I or II. In recrystallized domains of direction group III (e.g. domain A.B) only the basal plane with one dominant a-axis direction is available for intracrystalline slip. Slip in a conjugate sense occurs in the form of microshears along

inclined grain boundaries. Simultaneous grain boundary migration within these domains ensures that the inclined orientation of the conjugate grain boundary microshears is maintained. The inclination of grain boundaries, reflecting the shape preferred orientation of recrystallized quartz, is thus subject to a balance between passive deformation and grain boundary migration. The microstructure reflects the balance during the last strain increments.

In quartz, domainal fabrics with alternating c-axis orientation (herring-bone microstructures) reflect an alternating shear sense, i.e. a kinematic heterogeneity on the scale of a thin section. The observed tendency towards a preferred grain boundary alignment of the recrystallized grains subparallel to the c-axis orientation suggests that anisotropic diffusion properties of quartz may control the shape of the grains. Additionally, basal slip may favour the formation of deformation bands subparallel to the c-axis, i.e. tilting of the lattice along planes subparallel to the c-axis, as preserved in the non-recrystallized ribbon grain in domain B.E and the clast fragments. Subsequent transformation of these planes into grain boundaries and continuous grain boundary migration maintains their favourable orientation as grain boundary microshears (Fig. 13d), leading to formation of a stable fabric.

The asymmetry of the main slip direction (the a-axes maximum) with respect to the foliation plane is widely used as a shear sense indicator, the determination of the sense of shear being strictly valid only (i) if intracrystalline plasticity prevails (the analysed sample is more complex since grain boundary microshears also contribute to the deformation), (ii) if the foliation and the lineation clearly reflect the finite strain geometry, (iii) if the deformation is homogeneous from the thin section scale up to the shear zone (the analysed sample is not homogeneous) and (iv) under simple shear conditions (not observed in the sample) (i–iv after Law 1990). However, in many natural shear zones, strains are very high, and in many cases where the deformation is clearly one of simple shear, the angle between a-axis maximum and foliation is much too large in comparison to the amount of finite strain. In order to reconcile this discrepancy, Mancktelow (1987) and Schmid (1994) discussed the necessity of a second slip system on a bulk textural scale, but did not explicitly identify it. The model depicted in Fig. 13(d) is valid for plane strain: the combination of crystal plasticity (along the a-direction) grain boundary migration and grain boundary sliding processes (along the inclined grain boundaries) can accommodate simple shear without affecting the large angle between the dominant a-axis maximum and the shear zone boundary.

In this study, strain partitioning was found to be prevalent. Schmidt's easy glide hypothesis is valid for homogeneous fabrics. Since homogeneous fabrics are also found in deformed quartz veins, future studies will have to investigate under which conditions and by which mechanisms homogeneous fabrics may develop if they

evolve from a non-random initial fabric such as the one analysed here.

REFERENCES

Behr, H.-J. 1961. Beiträge zur petrographischen und tektonischen Analyse des sächsischen Granulitgebirges (mit Anlagenmappe). *Freiberger Forschungshefte* **C119**, 8–111.

Bouchez, J.-L. 1978. Preferred orientations of quartz <a> axes in some tectonites: kinematic inferences. *Tectonophysics* **49**, T25–T30.

Boullier, A. & Bouchez, J. -L. 1978. Le quartz en rubans dans les mylonites. *Bull. Soc. géol. France* **XX**, 253–262.

Drury, M. R. & Humphreys, F. J. 1988. Microstructural shear criteria associated with grain-boundary sliding during ductile deformation. *J. Struct. Geol.* **10**, 83–89.

Eisbacher, G. H. 1970. Deformation mechanics of mylonitic rocks and fractured granites in Cobequid Mountains, Nova Scotia, Canada. *Bull. geol. Soc. Am.* **81**, 2009–2020.

Etchecopar, A. 1977. A plane kinematic model of progressive deformation in a polycrystalline aggregate. *Tectonophysics* **39**, 121–139.

Fairbairn, H. W. 1949. *Structural Petrology of Deformed Rocks.* Addison-Wesley Press, Inc., Cambridge.

Fitz Gerald, J. D. & Stünitz, H. 1993. Deformation of granitoids at low metamorphic grade. I: Reactions and grain size reduction.. *Tectonophysics* **221**, 269–297.

Fueten, F., Robin, P.-Y. F. & Stephens, R. 1991. A model for the development of a domainal quartz c-axis fabric in a coarse-grained gneiss. *J. Struct. Geol.* **13**, 1111–1124.

Gapais, D. & Cobbold, P. R. 1987. Slip system domains. 2. Kinematic aspects of fabric developement in polycrystalline aggregates. *Tectonophysics* **138**, 289–309.

Garcia Celma, M. A. 1982. Domainal and fabric heterogeneities in the Cap de Creus quartz mylonites. *J. Struct. Geol.* **4**, 443–455.

Hobbs, B. E. 1966. Microfabric of Tectonites from the Wyangala. Dam Area, New South Wales, Australia.. *Bull. geol. Soc. Am.* **77**, 685–706.

Hobbs, B. E., Means, W. D. & Williams, P. F. 1976. *An Outline of Structural Geology.* Wiley International, New York.

Jessell, M. W. & Lister, G. S. 1990. A simulation of the temperature dependence of quartz fabrics. In: *Deformation Mechanisms, Rheology and Tectonics* (edited by Knipe, R. J. & Rutter, E. H.). *Geol. Soc. Spec. Publ. No.* 54, 353–362.

Knipe, R. J. & Law, R. D. 1987. The influence of crystallographic orientation and grain boundary migration on microstructural and textural evolution in an S-C mylonite. *Tectonophysics* **135**, 155–169.

Koark, H. J. 1957. Gefügeregel und Gefügegenität in einem Quarz in Quarz-B-Tektonit. *Bull. Geol. Inst. Uni. Uppsala* **XXXVII**, 43–79.

Kunze, K., Wright, S. I., Adams, B. L. & Dingley, D. J. 1993. Advances in automatic EBSP single orientation measurements. *Textures and Microstructures* **20**, 41–54.

Law, R. D. 1990. Crystallographic fabrics: a selective review of their applications to research in structural geology. In: *Deformation Mechanisms, Rheology and Tectonics* (edited by Knipe, R. J. & Rutter E. H.). *Geol. Soc. Spec. Publ.* 54, London, 335–352

Law, R. D., Schmid, S. M. & Wheeler, J. 1990. Simple shear deformation and quartz crystallographic fabrics: a possible natural example from the Torridon area of NW Scotland. *J. Struct. Geol.* **12**, 29–45.

Liniger, M. H. 1992. Der ostalpin-penninische Grenzbereich im Gebiet der nördlichen Margna-Decke (Graubünden, Schweiz). Ph. D. Thesis No. **9769**, ETH Zürich.

Linker, M. F. & Kirby, S. H. 1981. Anisotropy in the rheology of hydrolytically weakened synthetic quartz crystals. In: *Mechanical Behaviour of Crustal Rocks* (edited by Carter, N. L., Friedman, M. P., Logan, J. M. & Stearns, D. W). *Am. Geophys. Un. Geophys. Monogr.* **24**, Washington D. C., 29–48.

Linker, M. F. & Kirby, S. H. 1984. Effects of compression direction on the plasticity and Theology of hydrolytically weakened synthetic quartz crystals at atmospheric pressure. *J. geophys. Res.* **89**, 4241–4255.

Lister, G. S., Paterson, M. S. & Hobbs, B. E. 1978. The simulation of fabric development in plastic deformation and its application to quartzite: the model. *Tectonophysics* **45**, 107–158.

Lister, G. S. & Snoke, A. W. 1984. S-C Mylonites. *J. Struct. Geol.* **6**, 617–638.

Lister, G. S. & Williams, P. F. 1979. Fabric development in shear zones: theoretical controls and observed phenomena. *J. Struct. Geol.* **1**, 283–297.

Lloyd, G. E. & Freeman, B. 1991. SEM electron channelling analysis of dynamic recrystallization in a quartz grain. *J. Struct. Geol.* **13**, 945–953.

Lloyd, G. E., Law, R. D., Mainprice, D. & Wheeler, J. 1992. Microstructural and crystal fabric evolution during shear zone formation. *J. Struct. Geol.* **14**, 1079–1100.

Mainprice, D. & Nicolas, A. 1989. Developement of shape and lattice preferred orientations: application to the seismic anisotropy of the lower crust. *J. Struct. Geol.* **11**, 175–189.

Mancktelow, N. 1993. *StereoPlotXL 2.0.* ETH Zürich.

Mancktelow, N. S. 1987. Quartz textures from the Simplon fault zone, southwest Switzerland and north Italy. *Tectonophysics* **135**, 133–153.

Means, W. D. 1983. Microstructure and micromotion in recrystallization flow of Octachloropropane: A first look. *Geol. Rdsch.* **72**, 511–528.

Panozzo, R. H. 1983. Two-dimensional analysis of shape-fabric using projections of digitized lines in a plane. *Tectonophysics* **95**, 279–294.

Panozzo Heilbronner, R. & Pauli, C. 1993. Integrated spatial and orientation analysis of quartz c-axes by computer-aided microscopy. *J. Struct. Geol.* **15**, 369–382.

Panozzo Heilbronner, R. & Pauli, C. 1994. Orientation and misorientation imaging: integration of microstructural and textural analysis. In: *Textures of geological materials* (edited by Bunge, H. J., Siegesmund, S., Skrotzki, W. & Weber, K.). DGM Informationsgesellschaft mbH, Oberursel, 147–164.

Passchier, C. W. 1983. The reliability of asymmetric c-axis fabrics of quartz to determine sense of vorticity. *Tectonophysics* **99**, T9–T18.

Pauli, C. 1995. Quartz fabric domains: spatial and orientational analysis of microstructure and texture by computer integrated polarization microscopy. Ph.D. Thesis, University Basel.

Price, G. P. 1978. Study of heterogeneous fabric and texture within a quartz-feldspar mylonite using the photometric method. *Bull. geol. Soc. Am.* **89**, 1359–1372.

Ramsauer, H. 1941. Achsenverteilungsanalysen an Quarztektoniten. Ph.D. thesis, Innsbruck.

Sander, B. 1911. Über Zusammenhänge, zwischen Teilbewegung und Gefüge in Gesteinen. *Tschermaks Mineralogische und Petrographische Mitt.* **30**, 281 314.

Sander, B. 1930. *Gefügekunde der Gesteine.* Springer, Wien.

Sander, B. 1934a. Fortschritte der Gefügekunde der Gesteine Anwendungen, Ergebnisse, Kritik. Fortsch.. *Min. Krist. Petr.* **18**, 111–170.

Sander, B. 1934b. Petrofabrics (Gefügekunde der Gesteine) and orogenesis. *Am. J. Sci.* **153**, 37–50.

Sander, B. 1950. *Einführung in die Gefügekunde geologischer Körper, zweiter Teil: Die Korngefüge.* Springer, Wien.

Sander, B. 1970. *An introduction to the study of fabrics of geological bodies,* Engl. transl. Pergamon Press, Oxford.

Schaeben, H., Siemes, H., Höfler, S. & Will, G. 1990. Practical application of entropy optimization in quantitative texture analysis. In: *Deformation Mechanisms, Rheology and Tectonics* (edited by Knipe, R. J. & Rutter, E. H.). *Geol. Soc. Spec. Publ. No.*54, London, 375–381.

Schmid, S. M. 1994. Textures of geological materials: computer model predictions versus empirical interpretations based on rock deformation experiments and field studies. In: *Textures of geologic materials* (edited by Bunge, H. J., Siegesmund, S., Skrotzki, W. & Weber, K.). DGM Informationsgesellschaft mbH, *Oberursel* 279–301.

Schmid, S. M. & Casey, M. 1986. Complete fabric analysis of some commonly observed quartz c-axis patterns. In: *Mineral and Rock Deformation: Laboratory Studies* (edited by Hobbs, B. E. & Heard, H. C.). *Am. Geophys. Un. Geophys. Monogr.* **36**, Washington D. C., 263–286.

Schmid, S. M., Casey, M. & Starkey, J. 1981. An illustration of the advantages of a complete texture analysis described by the orientation distribution function (ODF) using quartz pole figure data. *Tectonophysics* **78**, 101–117.

Schmidt, W. 1926. Gefügesymmetrie und Tektonik. *Jb. geol. Bundesanst. (Wien)* **76**, 407–430.

Schmidt, W. 1927a. Untersuchung über die Regelung des Quarzgefüges kristalliner Schiefer. *Fortsch. Miner. Krist. Petrog.* **11**, 27–31.

Schmidt, W. 1927b. Zur Quarzgefügeregel. *Fortsch. Miner. Krist. Petrog.* **11**, 334–336.

Schmidt, W. 1932. *Tektonik und Verformungslehre*. Gebr. Borntraeger, Berlin.

Simpson, C. & Schmid, S. M. 1983. An evaluation of criteria to deduce the sense of movement in sheared rocks. *Bull. geol. Soc. Am.* **94**, 1281–1288.

Turner, F. J. & Weiss, L. E. 1963. *Structural analysis of metamorphic tectonites*. McGraw Hill Book Co., New York.

Wenk, H.-R. 1965. Gefügestudie an Quarzknauern und -lagen der Tessiner Kulmination. *Schweizerische Mineralogische Petrografische Mitteilungen* **45**, 467–515.

Wenk, H.-R., Canova, G., Molinani, A. & Kocks, U. F. 1989. Viscoplastic modeling of texture development in quartzite. *J. geophys. Res.* **94**, 17895–17906.